

Predicting wide binaries and deviations from standard gravity using machine learning algorithms

Amoy Ashesh,^{*} Harsimran Kaur,[†] and Sandeep Aashish[‡]

Department of Physics, Indian Institute of Technology Patna, Patna, Bihar 801106, India

(Dated: June 26, 2025)

We present a machine learning (ML) framework for the detection of wide binary star systems and the identification of deviations from standard gravity using Gaia DR3 data. By training supervised ML models on established wide binary catalogues, we efficiently classify wide binaries and employ clustering and nearest neighbour search to pair candidate systems. We recast the problem of identifying systematic deviations from standard gravity as a supervised anomaly detection. Our approach incorporates data preprocessing techniques such as SMOTE, correlation analysis, and PCA, and achieves high accuracy and recall in both binary classification and anomaly detection tasks. The resulting publicly available code enables rapid, scalable, and customizable analysis of wide binaries and gravitational anomalies, complementing conventional analyses and providing a valuable resource for future astrophysical studies.

I. INTRODUCTION AND MOTIVATION

Machine Learning (ML) has evolved into one of the most pivotal tools in the era of data intensive astronomy due to its efficiency and scalability, and is set to play a key role in the search for new physics in the coming decades. In recent literature, various studies have employed machine learning techniques to extract information from raw data which is otherwise difficult to analyse analytically and often computationally expensive. Stellar classification on the SIMBAD database was studied in Ref. [1], classification of accretion states of black holes was studied in Ref. [2], imposing constraints on the deviations from general relativity using ML in Ref. [3], the detection and parameter estimation process of

^{*} amoy.ashesh@gmail.com

[†] 05harsimran@gmail.com

[‡] aashish@iitp.ac.in

gravitational waves using ML was carried out in Ref. [4]. For an exhaustive summary of recent works in this directions, see Refs. [5–7].

In this paper, we take first steps to introduce machine learning assisted search for new physics in recently released Gaia DR3 dataset through primarily two sets of problems: (i) classification of wide binaries, and (ii) predicting deviations in the wide binaries. The former is among the well-known classification problems in astronomy, and extensively studied in literature using both traditional statistical methods [8–10] and machine learning techniques [1, 2, 7] in different contexts. The classification problem of wide binaries is interesting because these are gravitationally bound pairs of stars with large separations and can be used to study stellar evolution, dynamics, galactic structure as well as potential signatures of deviations from standard gravity [11]. Wide binary pairs of stars separated by thousands to tens of thousands of astronomical units operate precisely in the low-acceleration regime where modified gravity effects might emerge. Recent Gaia data releases have provided an unprecedented opportunity to study these systems across the Galaxy with high precision. However, identifying true gravitationally bound pairs and detecting subtle anomalies in their dynamics is complicated by noise, contamination and the scale of the dataset, thereby necessitating complex statistical analysis [8].

The latter is a relatively new problem and is rooted in the fact that despite the success of general relativity, there exist unresolved discrepancies at the galactic and cosmological scales invoking an increasing interest in modified theories of gravity, such as Modified Newtonian Dynamics (MOND) [12–16]. These theories predict measurable deviations from Newtonian gravity at extremely low accelerations, around $a_o \sim 10^{-10} m/s^2$ [9, 11, 17]. Wide binaries in the low acceleration regime are particularly sensitive to these deviations, as their dynamics can be significantly affected by modifications to standard gravity [11, 18, 19]. In fact, Chae [20, 21] has recently shown that a class of wide binary systems in the low-acceleration regime do exhibit systematic deviations from Newtonian gravity that is inconsistent with both dark matter and MOND based models. However, the methods for detecting these deviations often rely on probabilistic models and computationally intensive Markov Chain Monte-Carlo simulations, which struggle to scale with the increasing volume and complexity of astronomical data. Due to the relatively small number of deviating systems in an otherwise large dataset, we pose the problem of detecting deviations from gravity as the problem of anomaly detection in machine learning.

Anomaly detection technique in ML involves the detection of outliers or data points that show unexpected behaviour from the rest of the data. The conventional unsupervised anomaly detection assumes no labelled data; it relies on the assumption that anomalies are statistically different and rare compared to the majority of data. While more flexible, unsupervised methods may be less precise, especially in cases where small systematic deviations not clearly distinguishable from normal data appear [22]. Therefore, a supervised anomaly detection approach is adopted in this work because the dataset is very sparse, i.e., there are very few WBS systems in the raw data and there are very few deviations in the WBS catalogue, and it is proven in the literature [23] that unsupervised learning approaches do not perform satisfactorily with sparse datasets and require a labelled dataset approach to guide the model. In supervised anomaly detection, the model is trained on labelled data that includes both normal and anomalous instances, allowing it to learn clear distinctions between the two. This approach typically achieves higher accuracy when labelled anomalies are available, but can struggle in scenarios with rare or unseen anomalies.

We have employed a supervised ML approach to predict wide binaries and potential deviations from standard gravity. As is standard in any machine learning framework, various data preprocessing techniques like correlation analysis, Synthetic Minority Over-sampling Technique (SMOTE) and Principal Component Analysis (PCA) have been employed in this work. Confusion matrices and standard ML metrics have been used to analyse the performance of the models and tune the hyperparameters accordingly. We have also used the K-fold cross-validation technique for the anomaly detection problem. The codes used in this work are made available as a set of publicly available tools (hosted at <https://github.com/DespCAP/G-ML>) which can be used to generate a catalogue of wide binaries using our pre-trained models, and to get a rough estimate of anomalies without invoking the use of computationally expensive many-body Monte-Carlo simulations.

The structure of this paper is as follows. Sec. II outlines the essential machine learning tools and techniques including that of data preprocessing and evaluation of models. Sec. III describes the methodologies for using ML algorithms to predict wide binary pairs from the Gaia DR3 dataset. In Sec. IV we deal with the problem of detecting deviations from standard gravity as an anomaly detection problem. We conclude with few remarks and future outlook in Sec. V.

II. MACHINE LEARNING TECHNIQUES

The models are fitted onto a training dataset. The dataset utilized for prediction is called the testing dataset. The dataset was split into test and train cases in the ratio of 20: 80. The various Machine Learning models used are:

1. **Logistic Regression:** In machine learning, the Supervised Learning subcategory includes the commonly used algorithm of logistic regression. Its primary purpose is to predict the outcome of a dependent variable that belongs to a category based on a set of independent variables. This implies that the output must be categorical or discontinuous, such as Yes or No, 0 or 1, or true or false [24]. Nevertheless, rather than offering a precise value of 0 or 1, logistic regression generates probability values that fall within the range of 0 to 1.
2. **Decision Tree Classifier:** A supervised ML algorithm that is utilized primarily for classification tasks, although it can also solve regression problems. It operates on a tree-like structure that includes internal nodes representing the characteristics of a given data-set [25]. The branches denote the decision-making processes, and the leaf-nodes indicate the result. A DT comprises of two types of nodes: Decision Nodes, that possess multiple branches and are responsible for decision-making, and Leaf Nodes, which lack branches and represent the final decision or output. The Decision Tree arrives at its decisions or tests based on the properties or characteristics of the provided dataset.[25]
3. **Random Forest Classifier:** A supervised ML algorithm, helps classify the output variable as categorical or discontinuous. An RFC is based on ensemble learning, combining multiple decision trees to make more accurate predictions.[26] The algorithm creates a forest of DTs, each using a random subset (RSS). Each RSS has different features and data points. During the training process, the RFC randomly selects a subset of features, and the RSS creates a decision tree. This process is repeated several times to create multiple decision trees. [26] The algorithm predicts by aggregating each tree's predictions and choosing the class that receives the most votes. This approach helps to improve the accuracy and robustness of the model, as it reduces the impact of individual trees that may be overfitting the data. An RFC is often used for the

classification of images or text.

4. **K-Nearest Neighbors:** An ML algorithm used for the purposes of classification and regression. It falls under the category of supervised learning, meaning that it requires labelled data to train the model. It identifies new data-points on the basis of proximity to the k-nearest data-points in the training dataset [27]. The user determines the value of ‘k’ and ascertains the number of neighbours to consider. KNN is a non-parametric algorithm, meaning it makes no assumptions about the data distribution [27]. It is also easy to understand and implement, making it a popular choice for many classification and regression tasks. However, its performance can be affected by the choice of k, and it can be computationally expensive for large datasets.

5. **Support Vector Machine:** An ML algorithm, helps in tasks related to classification, regression, as well as outlier detection. It is a supervised learning algorithm; it thus requires labelled data to train the model. In SVM, the algorithm constructs a hyperplane (HP) in a High Dimensional Space (HDS) that may be deployed to separate the different classes in the data. [28] The objective is to ascertain the HP that maximises the margin, which is defined as the distance between the HP and the nearest data points of each class. Using the kernel trick (K-T) technique, SVM can handle both non-linearly and otherwise (linear) separable data (N-/LSD). The K-T transforms the input data into an HDS that can be LSD. SVM is particularly useful when dealing with high-dimensional data, for example, classifying images or text. It helps in handling datasets with a small number of samples, as it is less prone to overfitting compared to other algorithms. However, SVM may not be advisable for larger datasets and can be subject to the specific kernel function as well as other hyperparameters.[28] Nonetheless, with careful tuning of the parameters, SVM can be a powerful tool for solving many classification, regression, and outlier detection problems.

A. Evaluation Metrics

The accuracy, recall and F1 measure are evaluated on each ML algorithm. Confusion Matrices for all the algorithms were also plotted.

Accuracy is a metric used to determine the frequency with which a model accurately

predicts the outcome of a given task. It is indicated as the ratio of the correct predictions versus the overall predictions [29]. It is particularly useful when the classes in the data are evenly distributed.

Recall is a measure of how well the model identifies positive instances. To compute this metric, the sum of true positives is divided by that of true positives and false negatives [29]. It is a valuable metric for correctly identifying all positive instances, such as in medical diagnosis.

F1 measure is a combination of precision and recall, which provides a balance between these two metrics. This metric is determined by calculating the harmonic mean of precision and recall [29]. It considers false positives as well as false negatives. F1 measure is often deployed in binary classification problems when the data is imbalanced.

A confusion matrix is a tabular representation that is utilized to assess the effectiveness of a classification model (CM). It is a matrix that summarises the predicted and actual classifications of a model's output, providing a more detailed view of its performance than just a single accuracy score. A confusion matrix comprises four primary components that are utilised to assess the performance of a classification model. These components are true positives (TPs), false positives (FPs), true negatives (TNs), and false negatives (FNs). Each of them carries a specific meaning. TPs signify the number of instances where the CM accurately predicts the positive-class. FPs are the number of instances where the CM predicts the positive-class despite the actual class being negative. TNs signify the number of instances where the CM accurately predicts the negative-class. FNs correspond to the number of instances where the CM predicts the negative-class despite the actual class being positive [30].

B. Data Preprocessing

In data analysis and machine learning, having an imbalanced dataset can significantly impact the accuracy of the resulting predictions. In such cases, Synthetic Minority Over-sampling Technique (SMOTE) is a commonly used method to balance the dataset. SMOTE is a technique that generates synthetic data points for the minority class to balance the distribution of the classes in the dataset. This technique creates new observations for the minority class by using interpolation methods to create "synthetic" samples that are similar

to the existing minority class observations [31]. This process continues until the minority class has a representation similar to that of the majority class. By using SMOTE to balance the dataset, the resulting distribution of the classes is more even, which allows for more accurate predictions by machine learning models. This process can mitigate the issue of imbalanced classes and can lead to better results when working with imbalanced datasets. SMOTE, thereby, helps improve the accuracy of ML models when working with imbalanced datasets, and it is frequently used in data analysis and machine learning projects.

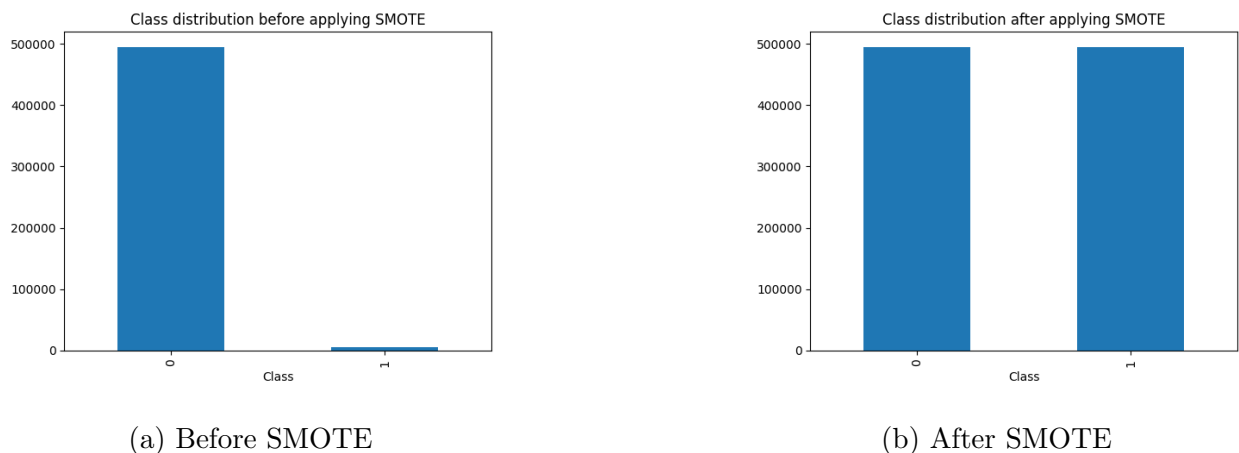


FIG. 1: Comparison of data distribution before and after applying SMOTE. Here 0 depicts that the entity is not a part of a WBS and 1 depicts that the entity is a part of a WBS.

All the ML models were trained on the SMOTE-balanced as well as the raw-filtered dataset. The ML models, once trained on the SMOTE-balanced dataset, were tested on the SMOTE-balanced test dataset and the raw-filtered test dataset. As depicted in FIG. 1, there was a significant increase in accuracy and other performance metrics corresponding to each ML model. The reason for the marked increase is that the raw-filtered dataset contains very sparse entries, and the desired classes have a stark distinction. Therefore, during the training process, the ML models inherently develop a bias towards the class with a higher occurring frequency and introduce redundancies that have to be countered by training the ML models on the class-balanced dataset using the SMOTE technique [31].

Correlation analysis has been employed to quantify the degree of linear association between two continuous variables. The Pearson correlation coefficient [32], denoted as r , has commonly been used for this purpose. It is defined as:

$$r = \frac{\sum_{i=1}^n (x_i - \bar{x})(y_i - \bar{y})}{\sqrt{\sum_{i=1}^n (x_i - \bar{x})^2} \sqrt{\sum_{i=1}^n (y_i - \bar{y})^2}},$$

where x_i and y_i represent individual data points, and \bar{x} and \bar{y} denote their respective means. The coefficient r ranges from -1 to 1 , indicating perfect negative correlation, no correlation, and perfect positive correlation, respectively.

Prior to computing the correlation coefficient, data sets were inspected for normality and linearity, as the Pearson metric assumes both. In cases where these assumptions were violated, the Spearman rank correlation coefficient [33], a non-parametric alternative, was used instead. This approach relies on ranked data and measures monotonic relationships, regardless of linearity.

Significance of the correlation has been assessed through hypothesis testing [34], with the null hypothesis assuming no correlation between the variables ($r = 0$). A two-tailed p-value has been calculated to determine whether the observed correlation differs significantly from zero, given the sample size.

Interpretation of correlation results has been guided by standard thresholds: values of $|r| < 0.3$ have been considered weak, $0.3 \leq |r| < 0.7$ moderate, and $|r| \geq 0.7$ strong [32].

Correlation analysis has provided insight into underlying relationships between physical parameters in the dataset, such as velocity dispersion, separation, and stellar mass, without implying causation.

C. Clustering and Nearest Neighbour Search

Once the set of all predicted WBS was obtained through the ML models, clustering was performed to reduce the sample size for the Nearest Neighbour Search. The K-Means clustering technique was used. K-means clustering partitions a dataset into k distinct, non-overlapping clusters by minimising the within-cluster sum of squares [35]. The algorithm initializes with k centroids and iteratively refines their positions by alternating between two steps: assignment of each point to the nearest centroid, and recalculation of centroid positions as the mean of all assigned points. The process converges when centroid positions stabilise or a maximum number of iterations is reached. K-means assumes clusters are spherical and approximately equal in size, which makes it sensitive to outliers and poorly suited for handling non-convex geometries or clusters with variable density. Moreover, the

choice of k must be specified a priori, often guided by heuristics such as the elbow method or silhouette score [35].

Nearest Neighbour Search (NNS) is a fundamental operation used to identify the closest data point(s) to a given query point in a defined feature space, based on a specific distance metric. It is widely used in applications such as classification, clustering, anomaly detection, recommender systems, and dimensionality reduction.

Given a dataset $\mathcal{D} = \{x_1, x_2, \dots, x_n\} \subset \mathbb{R}^d$ and a query point $q \in \mathbb{R}^d$, the goal of nearest neighbour search (NNS) is to find the point $x^* \in \mathcal{D}$ minimizing the distance to q , i.e., $x^* = \arg \min_{x \in \mathcal{D}} \text{dist}(q, x)$. Common choices for the distance function include Euclidean distance $\sqrt{\sum_{i=1}^d (q_i - x_i)^2}$, cosine distance $1 - \frac{q \cdot x}{\|q\| \|x\|}$, or other task-specific metrics [27]. While naive search requires $\mathcal{O}(n)$ comparisons and becomes expensive for large datasets, efficiency can be improved using methods like KD-Trees (in low dimensions), approximate nearest neighbour (ANN) techniques such as FAISS or HNSW (suitable for high-dimensional data), or locality-sensitive hashing (LSH) to reduce search complexity.

In this study, we apply NNS using 3D Euclidean distance to identify the nearest binary neighbour to each system. This enables us to examine local spatial clustering, detect potential hierarchical or contaminated systems, and provide local density information useful for unsupervised clustering methods like DBSCAN (future work). This spatial NNS is particularly useful in validating the independence of wide binaries in dynamical studies and ensuring that the dataset is not biased by unresolved associations or overlapping systems.

To identify local clustering or spatial associations among binary systems, we employ a nearest neighbour search (NNS) using the three-dimensional (3D) physical distance between binary pairs as the proximity metric. This method is useful for detecting local overdensities, potential contaminants (e.g., hierarchical triples or unbound co-moving pairs), and spatial coherence within a sample.

Given the 3D Cartesian positions (x, y, z) of stars derived from Gaia parallaxes and sky coordinates, the Euclidean distance between two stars A and B is calculated as:

$$D_{3D} = \sqrt{(x_A - x_B)^2 + (y_A - y_B)^2 + (z_A - z_B)^2}.$$

For each binary system, we search for its nearest neighbouring binary system in this 3D space. The resulting nearest neighbour distances provide a quantitative measure of local stellar density and can be used to flag potentially non-isolated binaries. The distribution of

nearest neighbour distances also informs selection criteria: binaries with anomalously small separations to other systems may be excluded or treated with caution, as they are more likely to be influenced by dynamical interactions or unaccounted-for hierarchical structure. In this study, the NNS results are further used in conjunction with clustering algorithms (e.g., DBSCAN) to confirm group memberships and validate the statistical independence of selected binary systems.

III. WIDE BINARY CLASSIFICATION PROBLEM

A. The wide binary catalogue

In a wide binary, both the components have the same age and composition which make them fit for astronomical analysis [8]. Moreover, due to their large separations, they help to understand the stellar disk formation in low-density areas [36]. While a wide binary is viewed as two point sources in the sky, chance alignment poses a challenge to the accurate identification of an authentic binary system. For years, the problem of increase in number of chance alignments with the increasing separation has been dealt with through different approaches like the inclusion of proper motion [37, 38] and using parallaxes and radial velocities [39]. The subsequent Gaia data releases [40–42] has revolutionized the construction of wide binary catalogues by dramatically increasing sample sizes and enabling more precise measurements of parallaxes and proper motions. Based on Gaia DR2 data, several catalogues were formed with different cuts on the separation and parallaxes [43–45]. Similarly, from the Gaia eDR3 dataset, wide binary catalogues have been generated in [8, 20]. The objective of our work is to predict wide binary pairs from raw Gaia DR3 dataset using a machine learning model trained on the existing catalogue in [8, 46].

This catalogue makes use of the Gaia eDR3 sources with parallaxes greater than 1 mas, fractional parallax uncertainties less than 20%, absolute parallax uncertainties less than 2 mas, and non-missing G-band magnitudes. The resulting dataset is then subjected to the following constraints:

1. Angular separation condition

$$\theta(/arcsec) \leq 206.265 \times \bar{\omega}(/mas) \quad (1)$$

where $\bar{\omega}$ is the parallax of the star with the brighter G magnitude and θ is the angle subtended by the arc connecting the two stars. The upper limit on the separation is called the Jacobi radius beyond which the Galactic tidal field becomes comparable to the gravitational attraction of the two stars and is given as $r_J \approx 1.35pc \times (\frac{M_{tot}}{M_o})$ (Binney et.al [47]).

2. Parallaxes consistent within 6 sigma:

El-Badry [8] gives the condition on the difference between the parallaxes to be consistent within 6σ , as it corresponds to the pairs with $\theta < 4$ arcsec and this angular separation is suitable for low chance alignment.

$$|\bar{\omega}_1 - \bar{\omega}_2| < 6\sqrt{\sigma_{\bar{\omega},1}^2 + \sigma_{\bar{\omega},2}^2} \quad (2)$$

where $\sigma_{\bar{\omega},i}$ is the parallax uncertainty of the i -th component.

3. Orbital proper motion:

Besides parallax, proper motion, i.e, the motion observed from Earth, also plays a vital role in determining the behaviour of a star/a system. The difference in the proper motion of the two stars are required to be consistent with a bound Keplerian orbit. This suggests that for a system of total mass $5M_o$, the projected velocity difference would be

$$\Delta\mu \leq \Delta\mu_{orbit} + 2\sigma_{\Delta\mu} \quad (3)$$

where

$$\begin{aligned} \Delta\mu &= [(\mu_{\alpha,1}^* - \mu_{\alpha,2}^*) + (\mu_{\delta,1} - \mu_{\delta,2})]^2]^{1/2} \\ \Delta\mu_{orbit}(mas/yr) &\leq 0.44(\bar{\omega}(mas))^{3/2}(\theta(arcsec))^{-1/2} \\ \sigma_{\Delta\mu} &= \frac{1}{\Delta\mu}[(\sigma_{\mu_{\alpha,1}}^* - \sigma_{\mu_{\alpha,2}}^*)\Delta\mu_{\alpha}^2 + (\sigma_{\mu_{\delta,1}} - \sigma_{\mu_{\delta,2}})\Delta\mu_{\delta}^2]^{1/2} \end{aligned} \quad (4)$$

Subsequent steps include dissolving clusters and cleaning the background to get unbound systems out of moving groups and star clusters, to finally generate the catalogue of labelled wide binaries.

B. Methodology

The objective is to predict whether a particular entry in the raw GAIA dataset is a part of WBS standalone or not (using ML), and further to generate pairs of WBS using Clustering

Techniques and Nearest Neighbour Search.

The catalogue chosen for marking the WBS is a subset of the El Badry catalogue. The code for generating the catalogue can be found in the following Zenodo repository: [Wide-binaries-from-Gaia-eDR3](#) [46] written for the paper "A Million WBS from GAIA eDR3" by El Badry et al. [8].

The workflow followed for the problem is outlined in FIG. 2.

The first step is the process of data extraction from the GAIA data archive. The data is then filtered and made into a catalogue of Wide Binary Systems (WBS) using Astronomical Data Query Language (ADQL). This task is achieved by systematically following the guidelines mentioned in the work done by Banik et al. [48]. The next step involves marking the obtained WBCs in the raw dataset. This is done so as to create a label that acts as the target variable of the ML model, and the other features in the dataset are the predictors that are used to train the ML model. The next step is the pre-processing and filtering of data to choose the optimal features for ML classification. The positional information, such as right ascension and declination, is intentionally taken out so as to avoid overfitting. After pre-processing, the task of implementing the ML model and performing accuracy measurements is carried out. According to the accuracy requirements, the hyperparameter values are tuned and the most optimal set is selected. Finally, the ML model is used to predict all the WBS in the dataset and then the WBS are paired together using clustering algorithms.

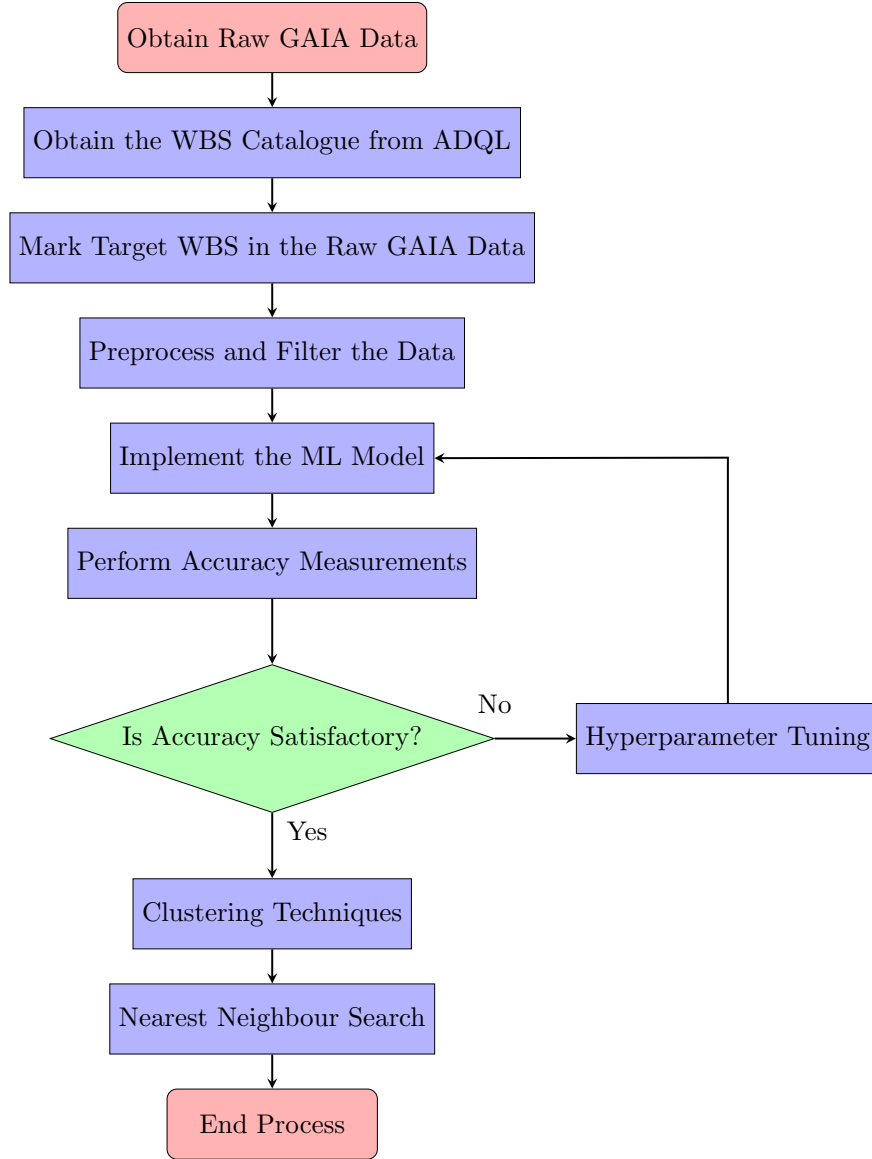


FIG. 2: Methodology for predicting WBS

The following was the flow of the program for the problem:

- (i) Loading: The first process is loading the raw data and the WBS catalogue. It is worth noting that this WBS catalogue, besides containing the raw features, also contains certain features that are obtained through statistical modelling, for example: 'pm1', 'pm2', 'pmra1', 'pmra2', 'pmdec1', 'pmdec2', 'pairedistance', 'sep_AU', 'binary_type'; and many others.
- (ii) Labelling: A set called "source_ids_set" is constructed from the 'source_id1' and 'source_id2' columns of the WBS catalogue. The "source_ids_set" is then mapped onto

the raw GAIA data to mark the WBS.

- (iii) Preprocessing: A check for NULL value containing columns was performed, and those columns were removed, and a filtered dataset was formed. A SMOTE balanced dataset was also generated from this filtered dataset to be used for training the ML models, along with the filtered dataset.

Additional steps that can be performed at this stage include: PCA reduction, correlation-based filtering: only including the most correlated features or setting some correlation cutoff.

- (iv) Implementation: The filtered and the SMOTE-balanced dataset were split into training and test datasets with a 80:20 ratio. The classes are skewed because the data is quite sparse. Therefore, there was a requirement for the SMOTE-balanced dataset to reduce the bias of the ML models during the training process and increase the accuracy and the number of true positives detected. The ML models were tested on the actual dataset to avoid introducing any bias in the system by SMOTE. A variety of ML algorithms were trained (some were trained only on the filtered dataset and not the SMOTE-balanced dataset): Random Forest Classifier (RFC), Logistic Regression (LR), Support Vector Machine with the Radial Basis Function (RBF) kernel (SVM_RBF), Decision Tree Classifier (DTC), K-Nearest Neighbour Classifier (KNN), Naive Bayes Classifier (NB), Bagging Classifier.

- (v) Evaluation: A threefold evaluation scheme was followed for every ML model: Firstly, the performance metrics were calculated for every model, including accuracy, precision, recall and F1 score. Secondly, the confusion matrices were calculated for every model. And lastly, another table depicting the accuracy of true positives was evaluated that contained the number of true positives, the true positive rate (%), the misclassification count and the misclassification rate (%).

- (vi) Clustering: Once the predictions from the ML model were obtained, the list of objects that were a part of a Wide Binary System was formed. This was the set of WBSs that had to be paired up with their companion stars. To efficiently handle the task of Nearest Neighbour Search and to reduce the computational complexity, clustering techniques were used to divide the data into discrete clusters, and then NNS was

performed on each of these clusters. K-Means clustering was performed on the features 'ra' and 'dec' (spatial distance) and 'parallax' (parallax distance). The number of clusters was set to 10.

- (vii) Nearest Neighbour Search: For each of the clusters, NNS was employed to efficiently search for the binary pairs. Given the 3D Cartesian positions (x, y, z) of stars derived from Gaia parallaxes and sky coordinates, the Euclidean distance between two stars A and B is calculated as:

$$D_{3D} = \sqrt{(x_A - x_B)^2 + (y_A - y_B)^2 + (z_A - z_B)^2}.$$

For each binary system, the search for its nearest neighbouring binary system in this 3D space was performed. The resulting nearest neighbour distances provide a quantitative measure of local stellar density and can be used to flag potentially non-isolated binaries.

C. Performance Report and Results

The SMOTE-balanced-trained ML models are expected to perform better because they reduce the inherent bias of the model due to the sparse dataset. Through TABLE I, it is clear that the SMOTE-balanced models perform much better than the base models.

More so, it is clear from TABLE II that there is an extremely high rate of misclassification in the base model, which is extremely reduced in the SMOTE-balanced dataset.

TABLE I: Performance metrics of the RFC algorithm on the raw-filtered dataset and SMOTE-balanced dataset for WBS detection

Algorithms	Precision	Recall	F1 score	Accuracy
RFC	0.375000	0.008234	0.016115	0.98901
RFC (SMOTE)	0.917273	0.923147	0.920201	0.99825

TABLE II: Classification Analysis of the RFC Algorithm on the raw-filtered dataset and SMOTE-balanced dataset for WBS detection

Algorithms	TP	TP rate (%)	Misclassifications	Misclassification rate (%)
RFC	9	0.823422	1099	100.548948
RFC (SMOTE)	1009	92.314730	175	16.010979

The confusion matrices also showcase the low detection rate of the base models, which is improved by the SMOTE-balanced models as observed in the FIG. 3a and FIG. 3b. A detailed plot for all the tested algorithms is given in the appendix A.



FIG. 3: Confusion matrices for the raw-filtered dataset predictions and the SMOTE-balanced dataset predictions

The clustering was performed with the total number of clusters set to ten. The nearest neighbour search was performed on each of the ten clusters to find the binary pairs.

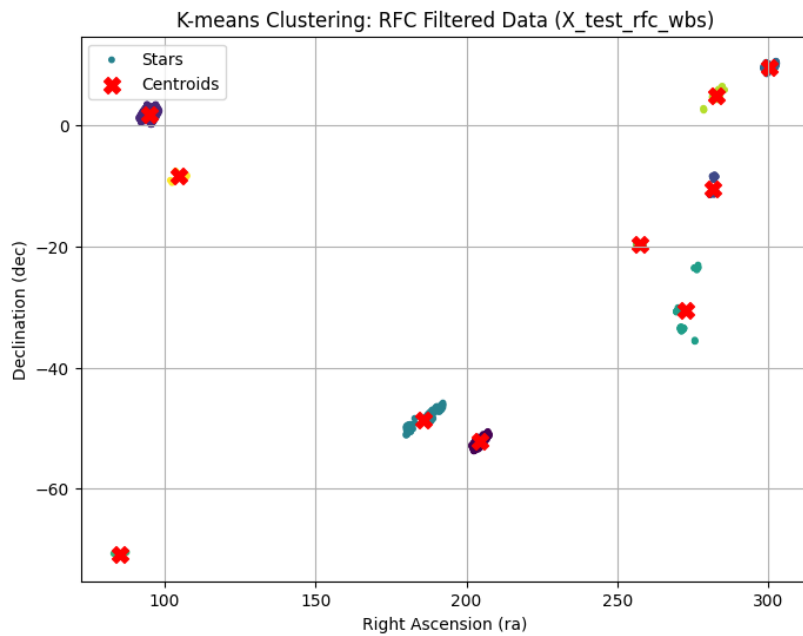


FIG. 4: The distribution of the clusters

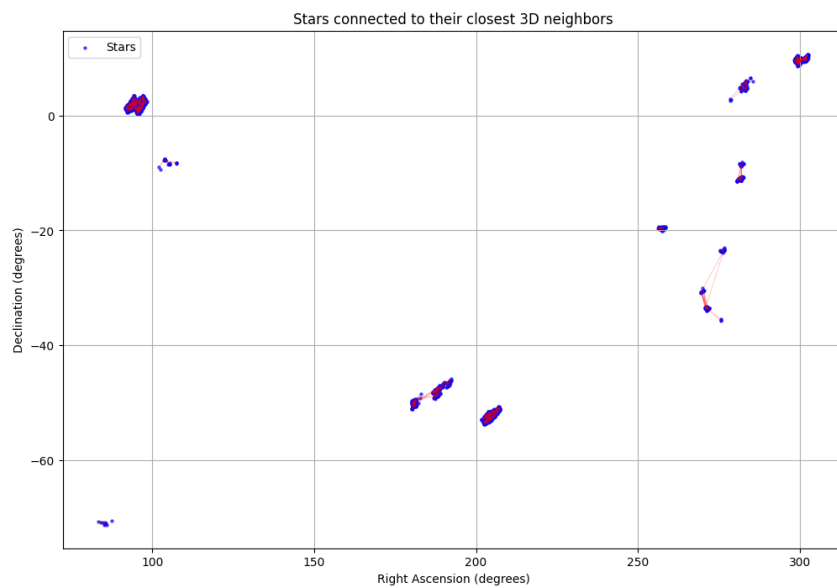


FIG. 5: WBS connected to their respective pairs

IV. DEVIATIONS FROM STANDARD GRAVITY AS AN ANOMALY DETECTION PROBLEM

A. Deviations from standard gravity

In context of machine learning, we treat the deviations from standard gravity as an anomaly detection problem for which we require a dataset to train the ML model. This dataset is another catalogue generated by Chae 2023 ([20]), based on El-Badry’s work.

This catalogue has the binary pairs that are within $80pc$ distance and $200pc$ distance separately from the point of observation. However, for the larger distance, measurement uncertainties increase, while for the smaller distance, the dataset is smaller in number. Moreover, all the binary pairs are of "MSMS" class. An "MS" type star can be a giant, a subgiant, a pre-main sequence star or a brown dwarf. Some other constraints of this catalogue are:

- $|d_A - d_B| < 3\sqrt{\sigma_{d_A}^2 + \sigma_{d_B}^2}$
- Relative errors of PM < 0.01
- Clean range $4 < M_G < 14$ and strict range $4 < M_G < 12$

Another feature of this catalogue which is of utmost importance in determining the parameter for the training of our ML model is the mass-magnitude relation. It associates the luminosity of the star with its mass using the spectroscopic and astrometric data like parallax, G-magnitude, photon flux and extinction coefficient. Pecaut and Mamjek 2013 [49] provides the mass-magnitude relation for the Chae’s sources along with masses, several colours and magnitudes for a wide range of spectral types in various wave bands in a tabulated format. However, [49] has made use of the GAIA DR2 observations, whereas, in this work we are dealing with the eDR3 quantities. Hence, the other band magnitudes from DR2 to the G-magnitude in eDR3 data have been transformed [20]. The first way is to transform the V-band magnitudes([50])

$$G - V = -0.01597 - 0.02809X_{VI} - 0.2483X_{VI}^2 + 0.03656X_{VI}^3 - 0.002939X_{VI}^4 \quad (5)$$

where $X_{VI} \equiv V - I_C$. The second option is to use the 2MASS J-band magnitudes

$$G - J = 0.01798 + 1.389X_{BR} - 0.09338X_{BR}^2 \quad (6)$$

where $X_{BR} \equiv BP - RP$.

[20]'s results gives a polynomial expression that effectively covers the sample selected in our work (clean range $4 < M_G < 14$ or strict range $4 < M_G < 12$), based on his outcome using a mass-magnitude relation.

The polynomial with the coefficients in V and J band is given as

$$\log_{10}\left(\frac{M_*}{M_o}\right) = \sum_{i=0}^{10} a_i (M_G)^i \quad (7)$$

coefficients	for M_V -based M_G	for M_J -based M_G
a_0	$5.2951695081428651 \times 10^{-1}$	$4.5004396006609515 \times 10^{-1}$
a_1	$-1.5827136745981818 \times 10^{-1}$	$-7.5227632902604175 \times 10^{-2}$
a_2	$8.48714785224177071 \times 10^{-3}$	$-1.6733691959840702 \times 10^{-2}$
a_3	$7.8449380571379954 \times 10^{-4}$	$3.2486543639338823 \times 10^{-3}$
a_4	$-5.2267549153639953 \times 10^{-5}$	$9.7481038895336188 \times 10^{-6}$
a_5	$-1.6957228195696253 \times 10^{-5}$	$-3.7585795718404064 \times 10^{-5}$
a_6	$1.6858627515537989 \times 10^{-6}$	$2.1882376017987368 \times 10^{-6}$
a_7	$-6.8083605428022648 \times 10^{-8}$	$-2.6298611913795649 \times 10^{-8}$
a_8	$1.4781005839376326 \times 10^{-9}$	$1.3151945936755533 \times 10^{-9}$
a_9	$7.7057036188153745 \times 10^{-11}$	$-9.3661053655257917 \times 10^{-11}$
a_{10}	$-4.4776519490406922 \times 10^{-12}$	$4.9792442749063264 \times 10^{-13}$

We consider the stars for analysis whose masses are $M_* < 1.2M_o$, where M_o is solar mass.

However, the masses of other objects outside the scope of this work can be obtained.

Since this work aims at training an ML model only, the resultant table from Chae ([20]), which is hosted at Chae Scripts [51] has been directly accessed in this work. Another way of finding the mass magnitude directly using the G-band magnitudes from the eDR3 data is by using the mass-luminosity relation given by Chevalier 2023 [52]. The Gaia DR3 data provides the G-band magnitudes for all the binary star systems (Gaia Collaboration 2023a [42]). The Gaia dust extinction law is useful in this case to determine the masses[53]. However, the outcome polynomial is applicable only for a limited range of stellar mass ($0.12 < M < 0.77$). As a conclusion, we draw that this method is applicable for our catalogue's range ($M \leq 1.2M_{\odot}$) if we extrapolate the polynomial or through some simulating methods. Thus, this deviates our work from the objective of training an ML model, and we follow the older method.

B. Labelling deviations

In the training of ML model, we intentionally eliminated the positional information so as to avoid any spatial bias. This elimination also hints at proposing a new parameter for anomaly detection, besides cutting down the computational cost.

In literature (Pittordis [18], Banik et al.[9]), the deviation from Newtonian gravity has been inferred using the \tilde{v} parameter. For the training of our ML model to identify anomalous systems, we employ this parameter as our primary input. \tilde{v} is given as

$$\tilde{v} = \frac{v_p}{\sqrt{GM_{tot}/s}} \quad (8)$$

v_p is the plane-of-sky velocity given as

$$v_p = 4.7404 \times 10^{-3} km/s \times \Delta\mu \times d \quad (9)$$

d is the distance in pc to the binary system and $\Delta\mu$ is the plane-of-sky proper motion given in section III A.

M_{tot} is the total mass of the system and s is the separation between the two stars.

While other authors have considered the projected components of the velocity and separation, we make use of the 2D plane-of-sky velocity(v_p) and the separation(s) estimated

while making the catalogue itself. This is due to the fact that we don't want to have a precise identification of a binary system that is deviating, but rather develop an anomaly detection system by a different approach. So to some extent, the uncertainties occurring are tolerable.

More recently, Chae([20]) has defined a new parameter using 'MCMC' simulations to show deviations and discarded the idea of \tilde{v} parameter, as the advent of projection effects makes it difficult to get correct \tilde{v} distribution.

For our work, however, we follow the method of Pittordis([18]) of \tilde{v} parameter because **(i)** for training an ML model, the computational cost is optimised and once the model is trained, the anomalies beyond our limits can also be calculated. **(ii)** Moreover, our model is trained on the MC realised results for Newtonian gravity(Chae[20]), thus we are aiming at more accurate results through the model.

To summarise, the MCMC procedure, being computationally expensive, is discarded. However, its results are used for the training of the ML model, which analyses the \tilde{v} parameters to give anomalies.

As a final step to this work, we found the \tilde{v} for the Newtonian simulated data points (extracted from a site mentioned in [20]) and the actual data points (of catalogue). We define a new parameter

$$\begin{aligned}\Delta\tilde{v} &= \tilde{v}_{New} - \tilde{v}_{obs} \\ \tilde{v}_{New} &= \frac{v_{New}}{\sqrt{GM/s}} \\ \tilde{v}_{obs} &= \frac{v_p}{\sqrt{GM/s}}\end{aligned}\tag{10}$$

The first step is to calculate the magnitude of the plane-of-sky relative proper motion:[20]

$$\Delta\mu_{rel} = \sqrt{(\mu_{\alpha,A}^* - \mu_{\alpha,B}^*)^2 + (\mu_{\delta,A} - \mu_{\delta,B})^2}.\tag{11}$$

where (α) and (δ) are the observed right ascension and the declination components of the proper motions (PMs) of the two components of a binary respectively, $(\mu_{\alpha,A}^*, \mu_{\delta,A})$ and $(\mu_{\alpha,B}^*, \mu_{\delta,B})$.

The magnitude of the plane-of-sky relative velocity is given by: [20]

$$v_p = 4.7404 \times 10^{-3} \text{ km s}^{-1} \times \Delta\mu_{rel} \times d,\tag{12}$$

where d is the distance in parsecs (pc) to the binary system, and all proper motion values are given in units of milliarcseconds per year (mas yr^{-1}). For d , we take the error-weighted mean of the distances to components A and B, denoted d_A and d_B , respectively. The value of the Newtonian circular velocity is given by: [20]

$$v_N = \sqrt{\frac{GM_{\text{tot}}}{s}} \quad (13)$$

where v_p is the projected velocity given by Equation (4), M_{tot} is the total mass of the system, s is the projected separation between the two components, and G is Newton's gravitational constant. The ratio of two projected quantities \tilde{v} is given by: [20]

$$\tilde{v} = \frac{v_p}{v_N}, \quad (14)$$

The \tilde{v} values of the actual data are compared with those of simulated values in a gravity theory (Newtonian gravity). A new parameter called delta (Δ_{dev}) given by:

$$\Delta_{dev} = \tilde{v}_{actual} - \tilde{v}_{newtonian} \quad (15)$$

The deviations lying outside $\pm 3\sigma$ of Δ_{dev} are marked as deviations in the actual dataset.

The following scheme was followed for determining deviations as mentioned in the analysis done by Chae et al., after a few modifications. [20]:

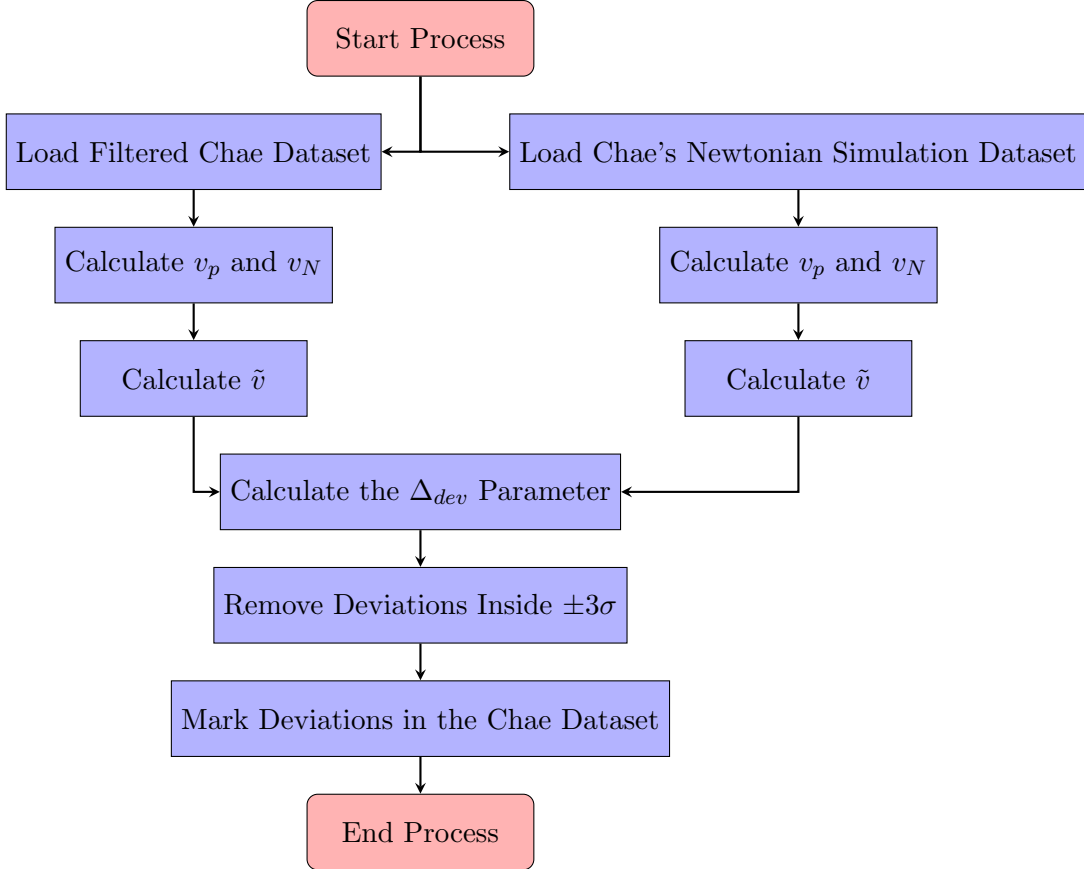


FIG. 6: Calculation flowchart

The deviations marked through the above-mentioned process are then used for training ML models.

C. Methodology

We use a supervised ML approach to identify gravitational anomalies present in the data, given a WBS catalogue. The WBS catalogue chosen for training the ML models was a subsection of the El Badry catalogue, generated by varying some of the given parameters to better estimate WBS. [46]. This catalogue was further filtered to only include the "SOURCE_ID"s of the WBS present in Chae's analysis. [20]

A supervised ML approach was followed for this task because the dataset is very sparse, and it is proven in the literature [23] that unsupervised learning approaches do not perform satisfactorily and require a labelled dataset approach to guide the model. A crude imple-

mentation of the unsupervised approach (Deep Neural Network) was also followed, but it was unable to identify the deviations.

For marking the deviations, the methodology mentioned in section IV B (Fig.6) was followed to obtain the deviating "SOURCE_IDs". This was achieved by using the data from 2 datasets: Chae's actual dataset and Chae's Newtonian simulation dataset. After the determination of the IDs, the ML best models were trained by marking the deviating IDs in the El Badry catalogue.

The best-trained ML models were then exported and used to predict deviating WBS in the entire El Badry catalogue. There is a provision for choosing the optimal model for predicting anomalies, namely, the most accurate model and the highest recall model. The most accurate model picks out the anomalies with the highest accuracy, while the highest recall model predicts almost all the anomalies, although it generates many false positives and is comparatively less accurate.

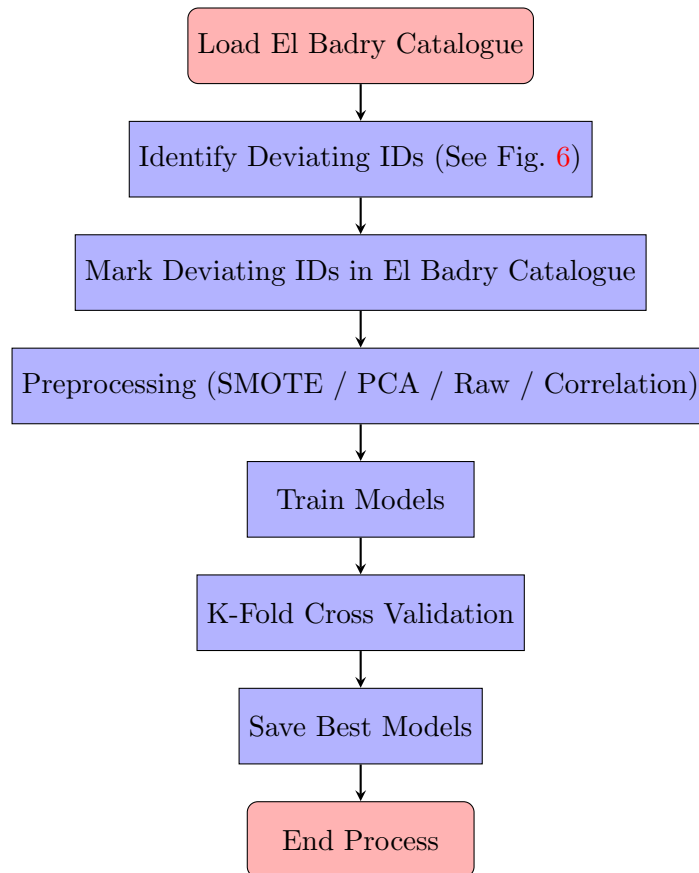


FIG. 7: Methodology for Predicting Deviations

The following was the flow of the program for the problem:

- (i) Loading: Three datasets have to be loaded - the modified El Badry catalogue, the Chae dataset and the Newtonian simulation Chae dataset. The training of the ML models would be performed on the modified El Badry catalogue. The other two would be used to determine the deviating IDs as mentioned in the section [IV B](#) (FiG.6).
- (ii) Identifying deviations: For both the Chae dataset and the Newtonian simulation Chae dataset, v_p , v_N , \tilde{v} and Δ_{dev} are calculated as mentioned in section [IV B](#). Deviations lying inside $\pm 3\sigma\Delta_{dev}$ are removed, and an additional cutoff is placed on the projection separation distance, which should be greater than 7 kAU. After imposing these constraints, the "SOURCE_ID"s of deviations are exported.
- (iii) Labelling: The exported IDs of the deviations from the previous step are matched with the El Badry catalogue and the deviations are marked in the El Badry Catalogue.
- (iv) Preprocessing: A check for NULL value containing columns was performed, and those columns were removed, and a filtered dataset was formed. The models were trained on the datasets that were preprocessed using the following techniques: correlation-based filtering, SMOTE, and PCA reduction. Correlation-based filtering techniques involve filtering out the uncorrelated or less correlated features to the target in the dataset. The two methods used for our model were to only include the most correlated features or to set a correlation cutoff on the features. The SMOTE-balanced dataset was generated from the filtered dataset to be used for training the ML models, along with the filtered dataset. The SMOTE-balancing was done to overcome the issue of class imbalances. The dimensionality of the data in the filtered dataset was reduced from 157 variables to 56, 10 and 13 (3 different PCA-reduced datasets) using PCA reduction on the filtered dataset, top correlation dataset and correlation cutoff dataset. A hybrid reprocessing combination of the above-mentioned techniques was also carried out to generate different datasets. Examples include SMOTE on correlation-filtered datasets and PCA on SMOTE-balanced datasets.
- (v) Training: A variety of differently preprocessed datasets and a variety of ML algorithms were used in the training phase. The data distributions are highly sparse for this

problem as well (refer to subsection IV A). Therefore, SMOTE was utilised to handle the class imbalances.

Several machine learning algorithms were trained including: Random Forest Classifier (RFC), Logistic Regression (LR), Support Vector Machine with a Radial Basis Function (RBF) kernel (SVM RBF), Decision Tree Classifier (DTC), K-Nearest Neighbors (KNN), Naive Bayes (NB), and the Bagging Classifier.

- (vi) K-Fold Cross Validation: The training dataset can be divided into k number of folds ($k = 5$ in our analysis). Different hyperparameter values for the Random Forest Classifier and the Balanced Random Forest Classifier with 3 different tuning methods. Firstly, in the accuracy tuning method, the hyperparameters that result in the most accurate model are selected. Secondly, in the F1 score tuning method, the hyperparameters that result in the model that gives the least number of misclassifications are selected. And lastly, in the recall tuning method, the hyperparameters that result in the model that predicts the most number of true positives are selected.
- (vii) Save Best Models: The best-performing models were saved, and the parameter files were exported. The user has the option to choose from the following two best models, since there is a trade-off between the number of true positives detected and the accuracy of the prediction: the most accurate model or the highest recall model. The most accurate model was a Random Forest Classifier trained on a dataset that was preprocessed to have a correlation cutoff value at 0.05. This means only the features/columns that have a correlation greater than this value were kept in the dataset, and the other features were not used for training. The model achieved an accuracy of 99.4759%. The highest recall model was a Balanced Random Forest Classifier, which was trained by k -Fold Cross Validation (5 folds) on a dataset that was preprocessed to have a correlation cutoff value at 0.05. The model had a true positive rate of 98.64%, although there was a reduction in accuracy because of the false positives.

D. Performance Report and Results

Many different models trained on differently preprocessed data were evaluated, and the best trained models are as follows:

- (i) **Most accurate models:** The model with the highest accuracy was a Random Forest Classifier (RFC) trained on a dataset that was preprocessed to have a correlation cutoff value at 0.05. The model achieved an accuracy of 99.4759%. Refer to TABLE III and TABLE IV for the performance metrics and the classification analysis, respectively.
- (ii) **Highest recall model:** The highest recall model was a Balanced Random Forest (BRF) Classifier, which was trained by k -Fold Cross Validation (5 folds) on a dataset that was preprocessed to have a correlation cutoff value at 0.05. The model had a true positive rate of 98.64%, although there was a reduction in accuracy because of the false positives. Refer to TABLE III and TABLE IV for the performance metrics and the classification analysis, respectively.

TABLE III: Performance Metrics of the most accurate model and the highest recall model (both trained on the correlation cutoff dataset) for anomaly detection

Algorithms	Precision	Recall	F1 score	Accuracy
RFC (most accurate)	0.838710	0.527027	0.647303	0.994759
BRF (highest recall)	0.105797	0.986486	0.191099	0.923788

TABLE IV: Classification Metrics of the most accurate model and the highest recall model (both trained on the correlation cutoff dataset) for anomaly detection

Algorithms	TP	TP rate (%)	Misclassifications	Misclassification rate (%)
RFC (most accurate)	78	52.702703	85	57.432432
BRF (highest recall)	146	98.648649	1236	835.135135

The confusion matrices also showcase the low detection rate of the base models, which is improved by the SMOTE-balanced models as observed in the FIG. 8a and FIG. 8b.

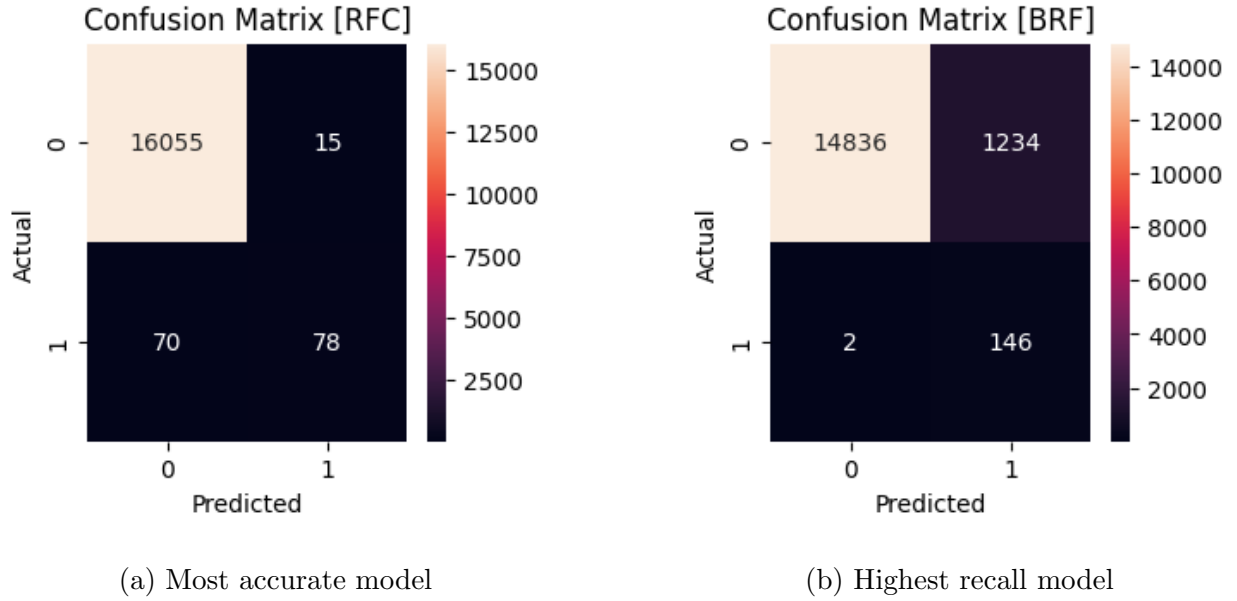


FIG. 8: Confusion matrices for the most accurate model and the highest recall model

There is a trade-off between the accuracy of the model and the number of deviations predicted/detected. Therefore, the choice of the model is left to the user according to their specific needs. The most accurate model predicts anomalies accurately, and hence it gives a list of deviations that are most likely true anomalies, as there are very few false positives. In contrast, the highest recall model predicts all the anomalies present in the dataset but there are a significant number of deviations.

V. CONCLUSIONS

We have applied machine learning (ML) techniques to the problems of detection of wide binaries and their potential deviations from standard gravity. Wide binary stars—stellar pairs separated by hundreds to thousands of astronomical units—are crucial astrophysical laboratories for testing gravitational theories, including potential deviations from Newtonian dynamics at large separations.

While conventional statistical techniques for detecting wide binaries are computationally expensive, relying on Monte-Carlo simulations and complex probabilistic analyses to rule out chance alignments, machine learning based approach offers a scalable alternative where techniques such as clustering algorithms and nearest neighbour search are used to efficiently

predict binaries from noisy background populations. In our implementation, the catalogue generated by El-Badry *et al.*[46] is the primary training dataset for the analysis of Sec. III. However the trained model can be used to predict pairs of a wide binary system directly from the raw Gaia DR3 data.

The second major focus of this work is detecting the recently reported systematic deviations from standard gravity in the low-acceleration limit of wide binaries [10, 20] by framing it as a supervised anomaly detection problem, aimed at identifying non-standard astrophysical systems, particularly deviations from Newtonian gravity. For this purpose, the catalogue and MCMC simulation data from Ref. [20] have been used as training data. Several supervised and semi-supervised learning models and varied preprocessing techniques like SMOTE, correlation-based filtering, PCA reduction, along with K-Fold Cross Validation were employed to uncover anomalies in the data.

Unlike the results of Ref. [20], however, we use a less accurate parameter \tilde{v} to quantify (and label) the deviations in the training data to avoid the computationally heavy step of obtaining 3D velocities through Monte-Carlo deprojections. To compensate for this, we use the Newtonian simulation results of Ref. [20] to train the models. However, it turns out the trained models do not rely on computationally complex algorithms like Markov Chain Monte Carlo (MCMC) simulations and can predict deviations very efficiently.

The publicly available tool (hosted at <https://github.com/DespCAP/G-ML>) developed as part of this work can be used to generate a catalogue of Wide Binary Stars quickly and fairly accurately from the raw GAIA source data. The type of ML model to be used and its hyperparameters, the kind of preprocessing techniques to be used, and clustering criteria are all tunable by the user. Our code also allows for tuning the marking process in the training phase, which enables the user to substitute a better alternative which can more accurately determine the deviations. Therefore, with the invocation of the ML algorithms, even computationally complex parameters (\tilde{v} here) can be used for training and then the trained model(s) can be used to predict without explicitly using the computationally complex parameters. There is also a provision of importing the pretrained model parameters so that the training phase is skipped, and the user can directly use the tool to predict WBS and make catalogues. The anomaly detection tool can be used to roughly determine the deviating systems from standard gravity, given a catalogue. The provision of importing the pretrained model parameters is available here as well. There are two pretrained options available to

the user: (i) the most accurate model or (ii) the highest recall model.

In summary, the program provides a list of WBS based on Raw GAIA data, without mapping them to their respective pairs. The trained model(s) can be directly used for predictions, which skips the training phase. The provision of a transfer-learning compatible solution ensures the ML training can be outsourced and used by a wider class of people. This automates the tedious analytical and statistical process of finding WBS systems.

We foresee several interesting directions that can be taken up as future problems, such as predicting deviations from the raw GAIA dataset and not the El-Badry catalogue, integrating and merging the repository on WBS predictions and anomaly detection on the raw GAIA data, expanding the models to predict more exotic and general gravitational phenomena or building an ML-based stellar object identifier for the GAIA data.

-
- [1] Seán Enis Cody, Sebastian Scher, Iain McDonald, Albert Zijlstra, Emma Alexander, and Nick Cox. Machine learning based stellar classification with highly sparse photometry data. *Open Research Europe*, 4:29, August 2024.
 - [2] H Sreehari and Anuj Nandi. A machine learning approach for classification of accretion states of black hole binaries. *Monthly Notices of the Royal Astronomical Society*, 502(1):1334–1343, January 2021.
 - [3] George Alestas, Lavrentios Kazantzidis, and Savvas Nesseris. Machine learning constraints on deviations from general relativity from the large scale structure of the universe. *Phys. Rev. D*, 106:103519, Nov 2022.
 - [4] Alexandra E Koloniari, Evdokia C Koursoumpa, Paraskevi Nousi, Paraskevas Lampropoulos, Nikolaos Passalis, Anastasios Tefas, and Nikolaos Stergioulas. New gravitational wave discoveries enabled by machine learning. *Machine Learning: Science and Technology*, 6(1):015054, February 2025.
 - [5] Dalya Baron. Machine learning in astronomy: a practical overview,, 2019.
 - [6] Mohammad H. Zhooldideh Haghghi. Analyzing astronomical data with machine learning techniques, 2023.
 - [7] Guangping Li, Zujia Lu, Junzhi Wang, and Zhao Wang. Machine learning in stellar astronomy: Progress up to 2024, 2025.

- [8] Kareem El-Badry, Hans-Walter Rix, and Tyler M Heintz. A million binaries from gaia edr3: sample selection and validation of gaia parallax uncertainties. *Monthly Notices of the Royal Astronomical Society*, 506(2):2269–2295, February 2021.
- [9] Indranil Banik and Hongsheng Zhao. Testing gravity with wide binary stars like α centauri. *Monthly Notices of the Royal Astronomical Society*, 480(2):2660–2688, October 2018.
- [10] Kyu-Hyun Chae. Robust evidence for the breakdown of standard gravity at low acceleration from statistically pure binaries free of hidden companions, 2023.
- [11] X. Hernandez, M. A. Jiménez, and C. Allen. Wide binaries as a critical test of classical gravity. *The European Physical Journal C*, 72(2), February 2012.
- [12] M. Milgrom. A modification of the Newtonian dynamics as a possible alternative to the hidden mass hypothesis. *Astrophys. J.*, 270:365–370, July 1983.
- [13] Mordehai Milgrom. Quasi-linear formulation of mond. *Monthly Notices of the Royal Astronomical Society*, 403(2):886–895, April 2010.
- [14] Kyu-Hyun Chae. Distinguishing dark matter, modified gravity, and modified inertia with the inner and outer parts of galactic rotation curves. *The Astrophysical Journal*, 941(1):55, dec 2022.
- [15] Robert Sanders. *Modified Gravity Without Dark Matter*, pages 375–402. Springer Berlin Heidelberg, 2007.
- [16] J. Bekenstein and M. Milgrom. Does the missing mass problem signal the breakdown of Newtonian gravity? *Astrophys. J.*, 286:7–14, November 1984.
- [17] Kareem El-Badry. The geometric challenge of testing gravity with wide binaries. *Monthly Notices of the Royal Astronomical Society*, 482(4):5018–5022, February 2019.
- [18] Charalambos Pittordis and Will Sutherland. Testing modified-gravity theories via wide binaries and gaia. *Monthly Notices of the Royal Astronomical Society*, 480(2):1778–1795, June 2018.
- [19] Charalambos Pittordis and Will Sutherland. Testing modified gravity with wide binaries in gaia dr2. *Monthly Notices of the Royal Astronomical Society*, 488(4):4740–4752, July 2019.
- [20] Kyu-Hyun Chae. Breakdown of the newton–einstein standard gravity at low acceleration in internal dynamics of wide binary stars. *The Astrophysical Journal*, 952(2):128, jul 2023.
- [21] Kyu-Hyun Chae. Measurements of the low-acceleration gravitational anomaly from the normalized velocity profile of gaia wide binary stars and statistical testing of newtonian and

- milgromian theories, 2024.
- [22] Srikanth Thudumu, Philip Branch, Jiong Jin, and Jugdutt Singh. A comprehensive survey of anomaly detection techniques for high dimensional big data. *Journal of Big Data*, 7(1):1–30, July 2020.
- [23] N. Goernitz, M. Kloft, K. Rieck, and U. Brefeld. Toward supervised anomaly detection. *Journal of Artificial Intelligence Research*, 46:235–262, February 2013.
- [24] D. R. Cox. The regression analysis of binary sequences. *Journal of the Royal Statistical Society: Series B (Methodological)*, 20(2):215–232, 12 2018.
- [25] Lior Rokach. Decision forest: Twenty years of research. *Information Fusion*, 27:111–125, 2016.
- [26] Leo Breiman. Random forests. *Machine Learning*, 45(1):5–32, 2001.
- [27] T. Cover and P. Hart. Nearest neighbor pattern classification. *IEEE Transactions on Information Theory*, 13(1):21–27, 1967.
- [28] Cortinna Cortes and Vladimir Vapnik. Support-vector networks. *Machine Learning*, 20(3):273–297, 1995.
- [29] Marina Sokolova and Guy Lapalme. A systematic analysis of performance measures for classification tasks. *Information Processing and Management*, 45(4):427–437, 2009.
- [30] Tom Fawcett. An introduction to roc analysis. *Pattern Recognition Letters*, 27(8):861–874, 2006. ROC Analysis in Pattern Recognition.
- [31] N. V. Chawla, K. W. Bowyer, L. O. Hall, and W. P. Kegelmeyer. Smote: Synthetic minority over-sampling technique. *Journal of Artificial Intelligence Research*, 16:321–357, June 2002.
- [32] Jacob Benesty, Jingdong Chen, Yiteng Huang, and Israel Cohen. *Pearson Correlation Coefficient*, pages 1–4. Springer Berlin Heidelberg, Berlin, Heidelberg, 2009.
- [33] Joost C. F. de Winter, Samuel D. Gosling, and Jeff Potter. Comparing the pearson and spearman correlation coefficients across distributions and sample sizes: A tutorial using simulations and empirical data. *Psychological Methods*, 21(3):273–290, September 2016.
- [34] Oona Rainio, Jarmo Teuho, and Riku Klén. Evaluation metrics and statistical tests for machine learning. *Scientific Reports*, 14(1):6086, March 2024.
- [35] T. Kanungo, D.M. Mount, N.S. Netanyahu, C.D. Piatko, R. Silverman, and A.Y. Wu. An efficient k-means clustering algorithm: analysis and implementation. *IEEE Transactions on Pattern Analysis and Machine Intelligence*, 24(7):881–892, 2002.
- [36] Ed J. Shaya and Rob P. Olling. Very wide binaries and other comoving stellar companions: A

- bayesian analysis of the hipparcos catalogue. *The Astrophysical Journal Supplement Series*, 192(1):2, dec 2010.
- [37] Julio Chaname and Andrew Gould. Disk and halo wide binaries from the revised luyten catalog: Probes of star formation and macho dark matter. *The Astrophysical Journal*, 601(1):289–310, January 2004.
- [38] Saurav Dhital, Andrew A. West, Keivan G. Stassun, and John J. Bochanski. Sloan low-mass wide pairs of kinematically equivalent stars (slowpokes): A catalog of very wide, low-mass pairs. *The Astronomical Journal*, 139(6):2566–2586, May 2010.
- [39] Jeff J. Andrews, Julio Chanamé, and Marcel A. Agüeros. Wide binaries in tycho-gaia: search method and the distribution of orbital separations. *Monthly Notices of the Royal Astronomical Society*, 472(1):675–699, August 2017.
- [40] Gaia Collaboration, A. G. A. Brown, and et al. Gaia data release 2. summary of the contents and survey properties. *Astronomy & Astrophysics*, 616:A1, August 2018.
- [41] Gaia Collaboration. Gaia early data release 3. summary of the contents and survey properties. *Astronomy & Astrophysics*, 649:A1, May 2021.
- [42] Gaia Collaboration, Arenou, F., and et al. Gaia data release 3 - stellar multiplicity, a teaser for the hidden treasure. *Astronomy & Astrophysics*, 674:A34, 2023.
- [43] Kareem El-Badry and Hans-Walter Rix. Imprints of white dwarf recoil in the separation distribution of gaia wide binaries. *Monthly Notices of the Royal Astronomical Society*, 480(4):4884–4902, 08 2018.
- [44] Hai-Jun Tian, Kareem El-Badry, Hans-Walter Rix, and Andrew Gould. The separation distribution of ultrawide binaries across galactic populations. *The Astrophysical Journal Supplement Series*, 246(1):4, January 2020.
- [45] Zachary D. Hartman and Sébastien Lépine. The superwide catalog: A catalog of 99,203 wide binaries found in gaia and supplemented by the superblink high proper motion catalog. *The Astrophysical Journal Supplement Series*, 247(2):66, April 2020.
- [46] Kareem El-Badry. Wide binaries from gaiaedr3. Zenodo, January 2021.
- [47] James Binney and Scott Tremaine. *Galactic Dynamics: Second Edition*. Princeton University Press, Princeton, NJ, 2008.
- [48] Indranil Banik, Charalambos Pittordis, Will Sutherland, Benoit Famaey, Rodrigo Ibata, Stefan Mieske, and Hongsheng Zhao. Strong constraints on the gravitational law from gaia dr3

- wide binaries. *Monthly Notices of the Royal Astronomical Society*, 527(3):4573–4615, November 2023.
- [49] Mark J. Pecaut and Eric E. Mamajek. Intrinsic colors, temperatures, and bolometric corrections of pre-main-sequence stars. *The Astrophysical Journal Supplement Series*, 208(1):9, September 2013.
- [50] M. Riello, F. De Angeli, D. W. Evans, P. Montegriffo, J. M. Carrasco, G. Busso, L. Palaversa, P. W. Burgess, C. Diener, M. Davidson, N. Rowell, C. Fabricius, C. Jordi, M. Bellazzini, E. Pancino, D. L. Harrison, C. Cacciari, F. van Leeuwen, N. C. Hambly, S. T. Hodgkin, P. J. Osborne, G. Altavilla, M. A. Barstow, A. G. A. Brown, M. Castellani, S. Cowell, F. De Luise, G. Gilmore, G. Giuffrida, S. Hidalgo, G. Holland, S. Marinoni, C. Pagani, A. M. Piersimoni, L. Pulone, S. Ragaini, M. Rainer, P. J. Richards, N. Sanna, N. A. Walton, M. Weiler, and A. Yoldas. Gaia early data release 3. photometric content and validation. *Astronomy & Astrophysics*, 649:A3, May 2021.
- [51] Chae and et al. Python scripts to test gravity with the dynamics of wide binary stars (Version v1), 2023.
- [52] S. Chevalier, C. Babusiaux, T. Merle, and F. Arenou. Binary masses and luminosities with gaia dr3. *Astronomy & Astrophysics*, 678:A19, 2023.
- [53] Danielski. Gaia dust extinction law, 2018.

Appendix A: Predicting WBS using ML

1. Data characteristics

The class distribution for the target column in the filtered dataset was:

```
y.value_counts()
0    494664
1     5336
```

The class distribution for the target column in the training and test datasets of the filtered dataset were:

```
y_train.value_counts()
```

```
0    395757
1     4243
```

```
y_test.value_counts()
```

```
0    98907
1     1093
```

The class distribution for the target column in the training dataset for the SMOTE-balanced dataset was:

```
re_y_train.value_counts()
```

```
0    396153
1    395309
```

2. Detailed plots and tables

TABLE V: Performance comparison of different ML algorithms on the raw-filtered dataset for WBS detection

Algorithms	Precision	Recall	F1 score	Accuracy
RFC	0.375000	0.008234	0.016115	0.98901
LR	0.000000	0.000000	0.000000	0.98907
SVM (RBF)	0.000000	0.000000	0.000000	0.98907
DTC	0.116667	0.134492	0.124947	0.97941
AdaBoost	0.400000	0.001830	0.003643	0.98906
KNN	0.000000	0.000000	0.000000	0.98907
NB	0.024346	0.086002	0.037949	0.95234
Bagging	0.222222	0.018298	0.033812	0.98857

TABLE VI: Performance Comparison of Machine Learning Algorithms with SMOTE balanced dataset for WBS detection

Algorithms	Precision	Recall	F1 score	Accuracy
RFC(SMOTE)	0.917273	0.923147	0.920201	0.99825
LR(SMOTE)	0.024428	0.086002	0.038049	0.95247
DTC(SMOTE)	0.668024	0.900274	0.766952	0.99402
AdaBoost(SMOTE)	0.061118	0.493138	0.108757	0.91166
KNN(SMOTE)	0.039785	0.867338	0.076080	0.76975
NB(SMOTE)	0.024093	0.085087	0.037553	0.95233
Bagging(SMOTE)	0.890291	0.838975	0.863872	0.99711

TABLE VII: Classification Analysis of ML Algorithms on the raw-filtered dataset for WBS detection

Algorithms	TP	TP rate (%)	Misclassifications	Misclassification rate (%)
RFC	9	0.823422	1099	100.548948
LR	0	0.000000	1093	100.000000
SVM (RBF)	0	0.000000	1093	100.000000
DTC	147	13.449222	2059	188.380604
AdaBoost	2	0.182983	1094	100.091491
KNN	0	0.000000	1093	100.000000
NB	94	8.600183	4766	436.047575
Bagging	20	1.829826	1143	104.574565

TABLE VIII: Classification Analysis of ML Algorithms with SMOTE balanced dataset for WBS detection

Algorithms	TP	TP rate (%)	Misclassifications	Misclassification rate (%)
RFC(SMOTE)	1009	92.314730	175	16.010979
LR(SMOTE)	94	8.600183	4753	434.858188
DTC(SMOTE)	984	90.027447	598	54.711802
AdaBoost(SMOTE)	539	49.313815	8834	808.234218
KNN(SMOTE)	948	86.733760	23025	2106.587374
NB(SMOTE)	93	8.508692	4767	436.139067
Bagging(SMOTE)	917	83.897530	289	26.440988

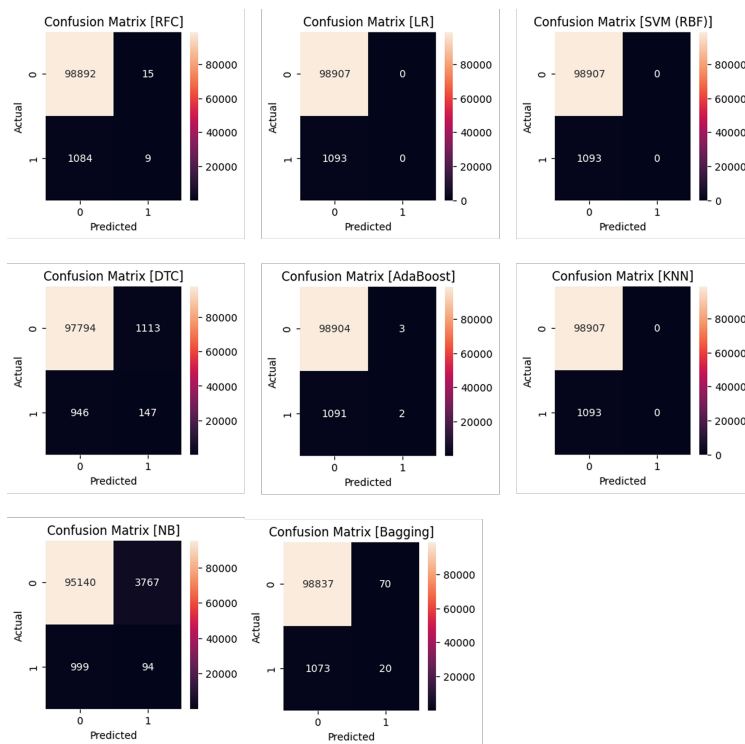


FIG. 9: CM for the raw-filtered dataset predictions

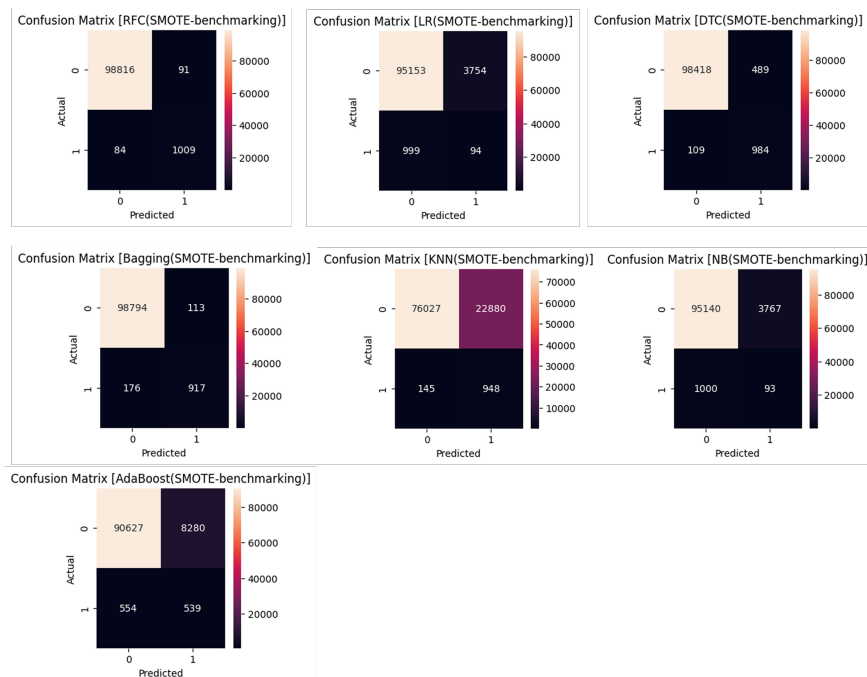


FIG. 10: CM for the SMOTE-balanced dataset predictions

Appendix B: Predicting anomalies using ML

1. Data characteristics

The class distribution in the filtered dataset was:

```
fdt['target'].value_counts()
0    80350
1     738
```

The class distribution for the target column in the training and test datasets of the filtered dataset were:

```
train['target'].value_counts()
0    64280
1     590
```

```
test['target'].value_counts()
0    16070
1     148
```

2. Detailed plots and tables

TABLE IX: Performance Comparison of the most accurate models (trained on correlation cutoff dataset)

Algorithms	Precision	Recall	F1 score	Accuracy
RFC	0.838710	0.527027	0.647303	0.994759
LR	0.000000	0.000000	0.000000	0.990874
SVM (RBF)	0.000000	0.000000	0.000000	0.990874
DTC	0.496933	0.547297	0.520900	0.990813
AdaBoost	0.752475	0.513514	0.610442	0.994019
KNN	0.000000	0.000000	0.000000	0.990874
NB	0.000000	0.000000	0.000000	0.990874
Bagging	0.824176	0.506757	0.627615	0.994512

TABLE X: Classification Metrics of the most accurate algorithms trained on the correlation cutoff dataset

Algorithms	TP	TP rate (%)	Misclassifications	Misclassification rate (%)
RFC	78	52.702703	85	57.432432
LR	0	0.000000	148	100.000000
SVM (RBF)	0	0.000000	148	100.000000
DTC	81	54.729730	149	100.675676
AdaBoost	76	51.351351	97	65.540541
KNN	0	0.000000	148	100.000000
NB	0	0.000000	148	100.000000
Bagging	75	50.675676	89	60.135135